

## The origin of the green color of variscite

GEORGES CALAS,<sup>1,\*</sup> LAURENCE GALOISY,<sup>1</sup> AND AMONMAT KIRATISIN<sup>1,2</sup>

<sup>1</sup>Laboratoire de Minéralogie-Cristallographie, UMR CNRS 7590, Universités de Paris 6 et 7 et Institut de Physique du Globe de Paris, Case 115, 75252 Paris Cedex 05, France

<sup>2</sup>Present address: Department of General Science, Srinakharinwirot University, Bangkok, Thailand

### ABSTRACT

The color of variscite from three different localities (Pannecé, France; Sarrabus, Sardinia; Ervedosa, Portugal) and metavariscite from Utah was investigated by diffuse reflectance and EPR spectroscopy. These samples contain low levels of transition elements such as V, Cr, and Fe, the relative concentration of which varies with origin, although they remain in the wt% range. The presence of peculiar antiresonance features indicates that octahedral Cr<sup>3+</sup> ions are responsible for the absorption bands that cause the green coloration of variscite and metavariscite. Trivalent iron ions, which give only a weak absorption band in some samples, and V<sup>3+</sup> ions do not contribute to the green coloration of the samples from these locations. The crystal-field splitting and B Racah parameter of Cr<sup>3+</sup> in variscite and metavariscite are 1590 and 657 cm<sup>-1</sup> and 1610 and 575 cm<sup>-1</sup>, respectively. These values indicate a weak crystal field and an important Cr-O covalence. Electron paramagnetic resonance spectra show the presence of minor amounts (300–500 ppm) of vanadyl groups substituted for Al. The absence of V<sup>3+</sup> indicates that variscite and metavariscite formed in an oxidizing environment.

### INTRODUCTION

Variscite and metavariscite, AlPO<sub>4</sub>·2H<sub>2</sub>O, are relatively rare hydrated aluminum phosphates which form at low temperatures as a result of phosphate-bearing surface solutions reacting with aluminum-rich rocks. They are usually deposited with other secondary phosphate minerals, such as apatite, wavellite, and crandallite, as a cementing material in various rocks, including schists, quartzite, or igneous rocks (Larsen 1942). Although the pure phases are white and transparent, variscite and metavariscite occur as beautiful green minerals with yellow to blue hues, and may be used as an ornamental stone. Because of their green color, they are sometimes confused with turquoise. Variscite has been used as an ornamental stone since the early Neolithic. Worked into beads and pendants as early as 4000 BCE, variscite jewels have been found in several parts of western Europe (Sheridan 2000), as in the Neolithic mines of Can Tintorer, Cataluna, Spain (Villalba 2002), and deposited in tombs throughout the megalithic fringe of Atlantic Europe, as at Carnac, French Brittany (Damour 1864).

The origin of the typical apple-green color of variscite and metavariscite is not clearly understood. Early qualitative studies, based on spectroscopic observations, indicated that the color was due to Cr<sup>3+</sup> (Anderson 1954, 1955, in Fritsch and Rossman 1987). However, the green color of variscite and metavariscite samples from Arkansas has also been attributed to the presence of small quantities of V<sup>4+</sup> and Cr<sup>3+</sup> (Foster and Schaller 1966). As noted by Marty et al. (1999), “the exact mechanism of coloration of variscite is still poorly understood.” The optical absorption spectrum of a variscite sample from Fairfield, Utah, suggested the presence of V<sup>3+</sup> (Rossman 2004). Such uncertainty arises

from the coincidental position of the absorption bands of V<sup>3+</sup> and Cr<sup>3+</sup> in several minerals, including garnets, spodumene, beryl, muscovite, etc. (Burns 1993). The variscite structure also accommodates other transition elements, such as ferric iron, and variscite forms a series with strengite, FePO<sub>4</sub>·2H<sub>2</sub>O. The fine-grained texture, with grain sizes reaching about 10 μm (Larsen 1942), limits our knowledge of the crystal chemistry of minor and trace components in these minerals. In the presence of associated impurity phases, such as ubiquitous Fe-oxides, it is necessary to use spectroscopic methods, which are sensitive only to transition elements located in a diamagnetic matrix. This manuscript presents the first comparative study of the spectroscopic properties of variscite and metavariscite. Diffuse reflectance spectroscopy is a convenient method to investigate crystal-field transitions in polycrystalline samples, as shown for Cr-bearing phyllosilicates (Calas et al. 1984). We have used this method, together with electron paramagnetic resonance (EPR), to show that Cr<sup>3+</sup> ions are responsible for the coloration of variscite and metavariscite samples from various localities with different concentrations of Cr and V. Similar absorption bands arising from Cr<sup>3+</sup> ions have recently been obtained from diffuse reflectance spectra of Neolithic variscite jewels from Western Europe (Galoisy et al. in prep.). The absence of V<sup>3+</sup> and the evidence of minor vanadyl groups indicate that oxidizing conditions prevailed during the formation of these low temperature minerals.

### SAMPLE DESCRIPTION

Variscite samples from three different localities and one metavariscite sample were selected on account of their range in Cr and V contents. Variscite samples from the stratabound polymetallic deposit at Sarrabus, Sardinia (Italy) have a pale green color, with no visible inclusions. Optical microscopy was

\* E-mail: calas@lmcp.jussieu.fr

used to confirm the homogeneity of the cryptocrystalline matrix of the samples used for spectroscopic study. Variscite from the Flocquerie quarry, Pannecé (France) occurs in fracture fillings within phanites of Silurian age (Forestier et al. 1973). These crystals have some visible narrow black veins included in a green cryptocrystalline matrix, the crystals of which are slightly larger than in the Sardinia sample. The variscite sample from Ervedosa, Portugal, comes from phosphate veins cutting Silurian metamorphic formations that were subsequently mineralized by cassiterite. They have an intense green color and are associated with turquoise (Meireles et al. 1987). Under the optical microscope the homogenous matrix is seen to be made up of tiny crystals, although larger crystals form a red-brown vein near the contact with the host rock. The metavariscite sample is from Fairfield, Utah, U.S.A. This mineral is also cryptocrystalline and shows no visible inclusions or dark veins. There is no evidence that these samples have been significantly altered since their initial crystallization and the optical properties and mineral crystal chemistry are thus expected to be of primary origin.

### EXPERIMENTAL METHODS

The mineralogical purity of the samples investigated in this study was previously checked using powder X-ray diffraction (XRD) and infrared spectroscopy. The chemical composition was obtained from polished thin sections by electron-probe microanalysis (EPMA) using a Cameca SX50 CAMEBAX microprobe equipped with four Wavelength Dispersive Spectrometers (WDS), operating at 15 kV and 40 nA. X-ray intensities were corrected for deadtime, background, and matrix effects using the Cameca PAP routine. The reference standards used were natural minerals and synthetic materials and included K-feldspar for Al, diopside for Si, MnTiO<sub>3</sub> for Ti and Mn, Fe<sub>2</sub>O<sub>3</sub> for Fe, apatite for P, vanadinite for V, and Cr<sub>2</sub>O<sub>3</sub> for Cr. For Al, Si, Fe, Mn, and Ti, the counting time was 15 s. The counting time was 10 s for P and 20 s for Cr and V. The analytical precision was about 1% relative under these conditions. Powder XRD patterns were obtained with a Philips PW1730 diffractometer using CoK $\alpha$  radiation (40 kV, 30 mA), operating in step-scan mode with a 0.04 $^{\circ}$ 2 $\theta$  step and counting 20 s per step.

Reflectance spectra were measured at room temperature between 4000 and 28 500 cm<sup>-1</sup> with a UV-Visible-NIR computerized CARY-5 spectrophotometer, fitted with a 114 mm diameter PTFE-coated integrating sphere and internal PMT and PbS detector. Flat, unpolished samples were held on a Teflon coated aluminum carrier. A blank sample (Halon) was measured prior to acquisition of each series of spectra. The spectral resolution varied from 1 nm in the UV region to 2 nm in the visible region. Diffuse reflectance values ( $R$ ) were obtained by reference to a Halon white standard ( $R = 100\%$ ). The Kubelka-Munk formalism was used to model the reflectance ( $R$ ) in the form of a remission function  $F(R)$ , which is a good approximation of the actual absorbance of a light scatterer of infinite thickness (see, e.g., Malengreau et al. 1994). In the Kubelka-Munk approximation (Hapke 1993),  $F(R)$  is related to the diffuse reflectance  $R$  by the relationship:

$$F(R) = \frac{(1 - R)^2}{2R} \quad (1)$$

$F(R)$  is used to quantify the optical absorption in samples that scatter light, as shown recently for chromium pigments (Pavlov et al. 2002) and vanadium oxide catalysts (Catana et al. 1998). The spectra were analyzed using Gaussian functions (Burns 1993) to represent the shape of the component bands, a procedure previously applied to diffuse reflectance spectra (Manceau and Calas 1985). The energy position of shoulders, well-defined, and narrow transitions was estimated with errors of 300, 100, and 30 cm<sup>-1</sup>, respectively.

Electron paramagnetic resonance experiments were done using a Bruker ESP300E EPR spectrometer operating at the X-band (9.42 GHz). The spectra were obtained at room temperature using calibrated silica tubes (Suprasil grade) under the following conditions: 100 kHz frequency modulation, 40 mW microwave power, and  $5 \times 10^{-4}$  T modulation amplitude. The magnetic field range was 0–0.9 T, calibrated relative to a DPPH standard ( $g = 2.0037 \pm 0.0002$ ). Frequency calibration was performed using a Hewlett-Packard frequency meter. The same volume of sample, accurately weighted, was used for each spectral measurement to minimize inaccuracies due to the variation of sensitivity with position in the EPR cavity.

## RESULTS

### Structural and chemical data

The diffraction patterns show that the variscite samples from the three locations correspond to the M-type crystal structure (Salvador-Salvador and Fayos 1972). Minor deviations from the reference cell parameters are due to the presence of substituted transition elements.

The various samples investigated show the presence of transition elements at or below the wt% level, the concentration of which is not correlated (Table 1). Iron is present in higher concentration in the variscite sample from Sardinia, as compared to the samples from Ervedosa and Pannecé. The metavariscite sample from Utah is almost Fe-free but is the richest in V. The variscite sample from Ervedosa shows a similar concentration of Cr, whereas the Cr content of Pannecé variscite and Utah metavariscite is smaller. The concentration of V in Ervedosa variscite is lower than in the other samples. These values are average values, as all samples show a distribution in the concentration of all transition elements.

### Optical absorption spectra

The remission function extracted from the diffuse reflectance spectrum of a variscite sample from Ervedosa, Portugal is shown in Figure 1, in the wavenumber range 6000–30 000 cm<sup>-1</sup>. The spectrum lies over a baseline characterized by an absorption which increases strongly at high wavenumbers. The sharp peaks at 6980 and 10 250 cm<sup>-1</sup> arise from overtones of OH vibrations of the structural water. The 6980 cm<sup>-1</sup> band is the first overtone of the OH stretch corresponding to the OH bond that is not involved in hydrogen bonding. On the high wavenumber side of the spectrum, the baseline has a steep slope due to a charge-transfer band, the origin of which will be discussed below. A small peak, located at approximately 23 500 cm<sup>-1</sup>, indicates the presence of Fe<sup>3+</sup> ions. Its position is different from that of the Fe<sup>3+</sup> absorption band in other phosphates such as phosphosiderite, FePO<sub>4</sub>·2H<sub>2</sub>O, which is isostructural with metavariscite (Rossman 1988). A weak, broad absorption band at around 11 000 cm<sup>-1</sup> extends from 9000 to above 13 000 cm<sup>-1</sup>. This band may be assigned to vanadyl groups, as octahedral Fe<sup>2+</sup> ions in phosphates such as vivianite, Fe<sub>3</sub>(PO<sub>4</sub>)<sub>2</sub>·8H<sub>2</sub>O, give rise to a more complex spectrum, with absorption bands near 1200 and 8000 cm<sup>-1</sup> (Amthauer and Rossman 1984).

The most important contributions to the remission function are two broad absorption bands of similar intensity located at

**TABLE 1.** Electron probe microanalysis of variscite and metavariscite (wt%)

	Ervedosa	Pannecé	Sardinia	Utah
Al <sub>2</sub> O <sub>3</sub>	29.4	29.1	28.2	29.3
SiO <sub>2</sub>	0.04	0.03	1.40	0.06
P <sub>2</sub> O <sub>5</sub>	45.3	44.7	44.3	44.4
TiO <sub>2</sub>	0.02	0.03	0.02	0.08
Fe <sub>2</sub> O <sub>3</sub>	1.50	0.15	2.00	0.05
V <sub>2</sub> O <sub>5</sub>	0.11	0.40	0.40	0.64
Cr <sub>2</sub> O <sub>3</sub>	0.40	0.20	0.30	0.14
MnO	0.03	0.05	0.02	0.03
H <sub>2</sub> O*	22.8	22.8	22.8	22.8
Total	99.6	97.46	99.45	97.5

\* The proportion of H<sub>2</sub>O was calculated by stoichiometry from the structural formula (22.81 wt% H<sub>2</sub>O).

15900 and 22500  $\text{cm}^{-1}$  and hereafter referred to as  $v_1$  and  $v_2$ , respectively. The  $v_1$  absorption band has a slightly asymmetric lineshape. The high wavenumber band,  $v_2$ , is broader than  $v_1$ , as usually observed in  $\text{Cr}^{3+}$ -bearing compounds. A weak feature located at about 21000  $\text{cm}^{-1}$  indicates splitting of the  $v_2$  transition. In octahedral coordination, the position of the  $v_1$  and  $v_2$  bands may correspond either to the  ${}^3T_{1g}(F) \rightarrow {}^3T_{2g}(F)$  and  ${}^3T_{1g}(F) \rightarrow {}^3T_{1g}(P)$  transitions of  $\text{V}^{3+}$  or to the  ${}^4A_{2g}(F) \rightarrow {}^4T_{2g}(F)$  and  ${}^4A_{2g}(F) \rightarrow {}^4T_{1g}(F)$  transitions of  $\text{Cr}^{3+}$  ions (Burns 1993). These bands cannot be used directly to determine the ion responsible for the green coloration of variscite. However, additional weak features on the low-wavenumber side of the  $v_1$  transition, around 15500 and 14500  $\text{cm}^{-1}$ , are assigned to spin-forbidden transitions of  $\text{Cr}^{3+}$  ions in a low crystal field,  ${}^4A_{2g}(F) \rightarrow {}^2E_g(G)$  and  ${}^4A_{2g}(F) \rightarrow {}^2T_{1g}(G)$  near 14500 and 15500  $\text{cm}^{-1}$ , respectively. As the  ${}^4A_{2g}$ ,  ${}^2E_g$ , and  ${}^2T_{1g}$  terms result from the same  $t_{2g}^3$  configuration, the bands corresponding to an electron jump between these states are expected to be sharp. In a weak crystal field, the spin-orbit coupling between  ${}^2E_g(G)$  and  ${}^2T_{1g}(G)$  with  ${}^4T_{2g}(F)$  levels results in antiresonance features (Lempicki et al. 1980; Pavlov et al. 2002) and produces specific dips instead of absorption bands on the sides of the band corresponding to the crystal field transition. The presence of two dips at 14620 and 14730  $\text{cm}^{-1}$  indicates a splitting of the  ${}^4A_{2g}(F) \rightarrow {}^2E_g(G)$  transition, which will be discussed below by comparison with metavariscite. The  $v_1$  and  $v_2$  bands may then be assigned to the  ${}^4A_{2g}(F) \rightarrow {}^4T_{2g}(F)$  and  ${}^4A_{2g}(F) \rightarrow {}^4T_{1g}(F)$  spin-allowed transitions of octahedral  $\text{Cr}^{3+}$  ions respectively. The only published optical absorption spectrum of a variscite sample from Fairfield, Utah, shows an absorption band at about 16000  $\text{cm}^{-1}$ , which was assigned to  $\text{V}^{3+}$  (Rossman 2004). The position of this band and the absence of these spin-forbidden transitions would indicate that the  ${}^3T_{1g}(F) \rightarrow {}^3T_{2g}(F)$  transition of  $\text{V}^{3+}$  in variscite occurs at the same wavenumber value as the  ${}^4A_{2g}(F) \rightarrow {}^4T_{2g}(F)$  transition of  $\text{Cr}^{3+}$ , the transmission window remaining at the same position.

Two other variscite samples, with a different relative proportion of V and Cr, have been investigated for comparison (Figs. 2b and 2c). The  $v_1$  and  $v_2$  bands remain at the same position and keep the same line width as the sample from Ervedosa,

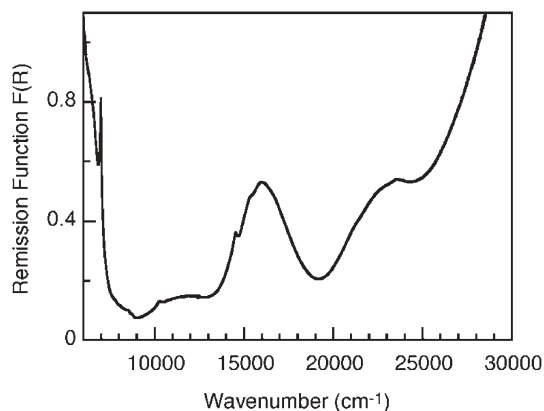


FIGURE 1. UV-visible and near-infrared diffuse reflectance spectrum of a massive variscite sample from Ervedosa, Portugal.

despite modification of the baseline. Of interest is the similarity of the position and relative intensity of the spin-forbidden transitions superimposed on the  $v_1$  transition. This indicates that only the  $\text{Cr}^{3+}$  ions contribute to the main absorption bands and are responsible for the green coloration of these variscite samples. The resolution of these transitions may vary among the samples due to slight differences in their crystallinity. These two samples show some differences in the high-wavenumber region. The small feature arising from ferric ions decreases in the order Sardinia, Ervedosa, to Pannecé, as does the total Fe content of the samples given by electron microprobe analysis (Table 1). These absorption bands are superimposed on a steep baseline, which is particularly apparent above 25000  $\text{cm}^{-1}$ . This rising absorption corresponds to ligand-to-metal charge transfer (LMCT) processes located in the near-UV. These bands cannot be resolved in diffuse reflectance spectra due to the limitations of diffuse reflectance spectroscopy in strongly absorbing samples. They may arise from  $\text{O} \rightarrow \text{V}$  charge transfer in vanadate and vanadyl groups, which causes an intense absorption in the near-UV (Catana et al. 1998; Frunza et al. 2000).  $\text{O} \rightarrow \text{Fe}^{3+}$  LMCT may also give an additional contribution in this spectral region, even with low contents of associated iron oxides (Malengreau et al. 1994).

The remission function of metavariscite (Fig. 2d) shows only minor differences from that of variscite. The most significant modification is the slight shift of the  $v_1$  absorption band toward higher wavenumbers, which occurs at 16100 and 15900  $\text{cm}^{-1}$  in metavariscite and variscite, respectively. The  ${}^4A_{2g}(F) \rightarrow {}^2E_g(G)$  and  ${}^4A_{2g}(F) \rightarrow {}^2T_{1g}(G)$  field-independent, spin-forbidden transitions characterize the presence of octahedral  $\text{Cr}^{3+}$  (see inset to Fig. 2). As the antiresonances remain at the same position as in variscite, they occur at a lower relative height on the low-wavenumber side of the  $v_1$  band. The  ${}^4A_{2g}(F) \rightarrow {}^2T_{1g}(G)$  transition has

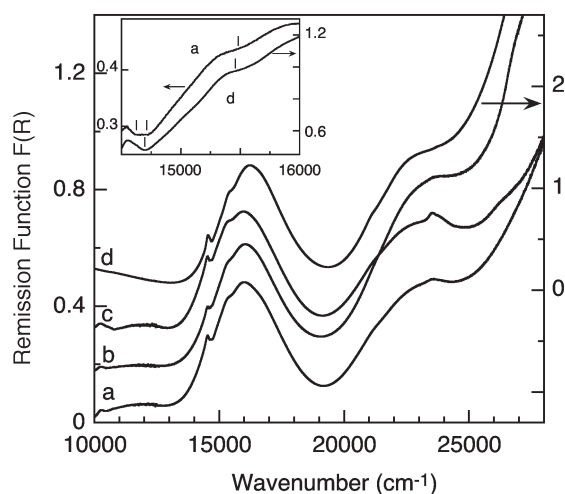


FIGURE 2. Diffuse reflectance spectra of massive variscite samples in the visible range. (a) Ervedosa; (b) Pannecé; (c) Sardinia; (d) metavariscite from Utah. The inset shows a detail of the spectrum of variscite and metavariscite. The dips correspond to the  ${}^4A_{2g}(F) \rightarrow {}^2E_g(G)$  and  ${}^4A_{2g}(F) \rightarrow {}^2T_{1g}(G)$  transitions near 14500 and 15500  $\text{cm}^{-1}$ , respectively. A noteworthy difference exists between the values of the remission function of variscite and metavariscite, on the left and right ordinate scale, respectively.

the same low intensity as in variscite, as the  ${}^4A_{2g}(F) \rightarrow {}^2E_g(G)$  transition is not split, an indication of a different local symmetry for Cr between variscite and metavariscite. The v2 band lies on the tail of an intense charge-transfer band and occurs near 22 100  $\text{cm}^{-1}$ . The contribution from diluted  $\text{Fe}^{3+}$  ions at about 23 500  $\text{cm}^{-1}$  is hardly visible. As Fe is almost absent (Table 1), and the EPR spectra do not show the presence of vanadyl groups, the intense absorption in the UV range may arise from the tail of a LMCT band ( $\text{O} \rightarrow \text{V}$ ) from vanadate groups, as electron microprobe analyses indicate a high V content (0.64 wt%  $\text{V}_2\text{O}_5$ ).

### Electron paramagnetic resonance (EPR) spectra

In addition to  $\text{Cr}^{3+}$  transitions at low field values, an indication of low-symmetry  $\text{Cr}^{3+}$  site distortion (Balan et al. 2002), the EPR spectrum of Pannecé variscite shows, near  $g = 2$ , a set of 8 parallel and 8 perpendicular lines, superimposed on a broad contribution (0.6 T) (Fig. 3a). This signal, centered at about 0.34 T, is assigned to axially distorted  $\text{V}^{4+}$  centers, in which the single unpaired electron interacts with the nuclear spin  $I = 7/2$  of  ${}^{51}\text{V}$  (natural abundance of  ${}^{51}\text{V} = 99.76\%$ ). In the typical spectrum of isolated  $\text{V}^{4+}$  centers, the parallel and perpendicular structures are well resolved but overlapping. This spectrum can be described by the following axially symmetric spin Hamiltonian  $H$  (Calas 1988):

$$H = \beta(g_{\parallel}B_zS_z + g_{\perp}(B_xS_x + B_yS_y) + A_{\parallel}I_zS_z + A_{\perp}(I_xS_x + I_yS_y)) \quad (2)$$

where  $\beta$  is the Bohr magneton,  $B_z, B_x, B_y$  are the components of the magnetic field,  $S_z, S_y, S_x$  and  $I_z, I_x, I_y$  are the components of the spin operators of the electron and the nucleus, respectively,  $g_{\parallel}$  and  $g_{\perp}$  are the spectroscopic splitting factors parallel and perpendicular to the magnetic field, respectively, and  $A_{\parallel}$  and  $A_{\perp}$  are the corresponding hyperfine splitting constants. The magnitude

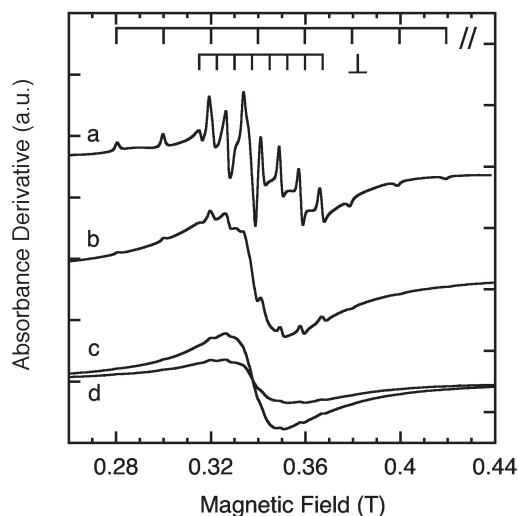


**FIGURE 3.** EPR spectrum of  $\text{V}^{4+}$  in variscites from (a) Pannecé, (b) Ervedosa, (c) Sardinia, and (d) metavariscite from Utah. The position of the parallel and perpendicular hyperfine components is indicated at the top.

of  $A_{\parallel}$  and  $A_{\perp}$  depends on the strength of the hyperfine coupling between the unpaired electron and the  ${}^{51}\text{V}$  nucleus and is then related to the ionicity of the V-O bond. The  $z$ -axis corresponds to the main axis of the axially symmetric  $g$  and  $A$  tensors.

The center of each group of 8 transitions and the spacing between them is determined by the values of the  $g$  factor and hyperfine structure factor, respectively. The values of the EPR parameters of  $\text{V}^{4+}$  in variscite are reported in Table 2 and indicate an octahedral symmetry. The  $g$  tensor of  $\text{V}^{4+}$  exhibits an axial symmetry, with  $g_{\parallel} > g_{\perp}$ , an indication of the formation of a compressed  $\text{V}^{4+}\text{-O}$  bond. By comparison with the EPR studies of V-bearing kaolinites (Muller et al. 1995), the  $\text{V}^{4+}$  concentration may be estimated to be in the range 300–500 ppm. This value indicates that this oxidation state corresponds to a minority of the V present in the sample.

The EPR spectra of the two other variscites and metavariscite samples show different contributions of the two components. These are characterized by a broad signal centered at the same position as the most intense hyperfine contribution, due to the almost coincidence of the parallel and perpendicular  $m_i = -1/2$  transitions (see Fig. 3a). The apparent  $g$  value, 2.004, is close to that of the free electron ( $g = 2.0023$ ). The width of this signal is 0.027, 0.021, and 0.025 T for the Ervedosa and Sardinia variscite and metavariscite, respectively. There is a weak superimposed signal due to the hyperfine structure of isolated vanadyl groups, which corresponds to the same EPR parameters as in the Pannecé sample. The central hyperfine transitions almost completely disappear, but the outermost perpendicular components are still visible. The intensity of the total EPR spectrum and of the hyperfine components decreases in the order Ervedosa, Sardinia, Utah (Figs. 3). The latter has an almost structureless symmetric lineshape, which cannot arise from associated superparamagnetic Fe-oxides in a sample in which Fe is almost absent (Table 1). Unresolved hyperfine coupling arises from dipolar broadening or strong exchange interactions between adjacent electron spins, an indication of some clustering of paramagnetic impurities in the lattice of these samples. A strong coupling averages out the hyperfine interaction with the vanadium nucleus and leads to a smearing out of some components of the hyperfine structure. Similar spectra have been found in vanadyl phosphate catalysts (Ruitenbeek 1998) and class II mixed valence complexes (Babonneau et al. 1982; Gupta et al. 1995). The weak optical absorption in the 12 000–15 000  $\text{cm}^{-1}$  region confirms the low concentration of vanadyl groups in variscite. The broad  $g \approx 2$  resonance may however be enhanced by additional interactions involving  $\text{Cr}^{3+}$  ions, such as Cr-Cr and Cr-V interactions, which may explain the increasing contribution of this broad component as the Cr content of variscite increases.

**TABLE 2.** EPR parameters of selected V species

Compound/host lattice	$g_{\parallel}$	$g_{\perp}$	$A_{\parallel}$	$A_{\perp}$	Reference
Variscite	1.926	1.978	18.2	7.1	This study
$\text{VO}(\text{H}_2\text{O})_5^{2+}$	1.933	1.980	18.2	7.1	Ballhausen and Gray (1962)
$\text{AlPO}_4\text{:V}$	1.935	1.974	18.3	6.6	Frunza et al. (2000)
$\text{ZnNH}_4\text{PO}_4 \cdot 6\text{H}_2\text{O}:\text{VO}^{2+}$	1.929	1.979	20.0	8.0	Shiyamala et al. (2002)
$\text{V}^{4+}$ in $\text{GeO}_2$ (tetragonal)	1.929	1.976	17.6	6.8	Siegel (1964)
$\text{V}^{4+}$ in $\text{GeO}_2$ (hexagonal)	1.963	1.921	13.4	3.7	Siegel (1964)*

\* Tetrahedral  $\text{V}^{4+}$ .

## DISCUSSION

### The origin of the green coloration of variscite and metavariscite

A major characteristic of the diffuse reflectance spectra of variscite and metavariscite is the presence of peculiar antiresonances, which are due to  $\text{Cr}^{3+}$  spin-forbidden transitions. These antiresonances are not observed in optical absorption spectra of  $\text{V}^{3+}$  in minerals. Indeed, this would correspond to a crossing between the  ${}^1E_g(D)$  and  ${}^1T_{2g}(D)$  levels and the  ${}^3T_{2g}(F)$  level, predicted at a  $Dq/B$  ratio of 17, where  $B$  is the Racah parameter and  $Dq$  is derived from the crystal field splitting parameter  $10Dq$ . The actual  $Dq/B$  ratio determined from the optical absorption spectra of  $\text{V}^{3+}$  in minerals is higher than this value and ranges from 28 to 45, using  $Dq$  and  $B$  values from the literature (Burns 1993). Trivalent chromium is then the only transition element to give rise to electronic  $d-d$  transitions responsible for all the absorption bands observed in the samples investigated. The crossing between the  ${}^4T_{2g}(F)$  and the  ${}^2E_g(G)$  and  ${}^2T_{1g}(G)$  field independent levels causes antiresonance features, which are seen as dips superimposed on the v1 transition and confirm the assignment to octahedral  $\text{Cr}^{3+}$ . The apple-green color of variscite results from the transmission window, which lies between the v1 and v2 absorption bands and is located at about  $19\,000\text{ cm}^{-1}$ . This transmission window is slightly shifted to  $19\,300\text{ cm}^{-1}$  in metavariscite. The same absorption bands arising from  $\text{Cr}^{3+}$  ions have recently been observed in diffuse reflectance spectra of Neolithic variscite jewels from Western Europe (Galoisy et al. in prep.).

The  $\text{Cr}^{3+}$  bands are more intense by a factor 3 in metavariscite than in variscite. According to the Kubelka-Munk formalism, the remission function depends on the absorption coefficient  $k$  and the scattering factor  $s$ :

$$F(R) = \frac{(1-R)^2}{2R} = \frac{k}{s} \quad (3)$$

The modification of the color purity may either arise from a different concentration of the coloring ion or from variations in the size of the scattering domains (Hapke 1993). As the Cr-concentration is lower in metavariscite than in the variscite samples investigated, the inverse relationship between  $F(R)$  and  $s$  indicates that an enhanced light absorption is due to a smaller light scattering in metavariscite, in relation to a larger size of the scattering domains. The efficiency of the scattering factor may explain the visual influence of the aging of historic lapidary remains of variscite. Some samples lose their coloration by exposure to the sun or after heating at  $60\text{ }^\circ\text{C}$  for 2 days, due to the transformation of variscite into metavariscite (Garcia-Guinea et al. 2000). This apparent bleaching may arise from a decrease in the size of the scattering domains during the phase transformation.

### Crystal chemistry of $\text{Cr}^{3+}$

In the variscite structure the  $\text{AlO}_4(\text{H}_2\text{O})_2$  octahedra are slightly distorted. They are corner-linked to four adjacent  $\text{PO}_4$  tetrahedra, with the two water molecules in a cis-position, and build chains of alternating octahedra and tetrahedra linked to form a three-dimensional framework. Al-O distances range between 1.856 and 1.899 Å for the O atoms belonging to  $\text{PO}_4$  groups and are shorter than the Al-O distances relative to the two water molecules,

1.909 and 1.963 Å (Kniep et al. 1977). In metavariscite (Kniep and Mootz 1973), Al-O distances are slightly smaller and less distributed, in the range 1.859–1.888 Å and 1.892–1.953 Å for the O atoms belonging to  $\text{PO}_4$  and  $\text{H}_2\text{O}$ , respectively.

The optical absorption bands are characteristic of  $\text{Cr}^{3+}$  in near octahedral symmetry, an indication that these ions replace  $\text{Al}^{3+}$  in variscite and metavariscite. The v1 band shows a slight asymmetric shape, without apparent splitting. Therefore, we may interpret the spectrum on the basis of an effective local crystal field with  $O_h$  symmetry. For a  $d^3$  electron configuration and octahedral coordination, the value of the v1 transition is equivalent to the crystal field splitting parameter  $10Dq$ . The crystal field splitting parameter  $Dq$  is slightly higher in metavariscite than in variscite, 1610 and  $1590\text{ cm}^{-1}$ , respectively, and the average Cr-O distances are smaller by 0.01 Å in the former. As these crystal field variations reflect size differences between the host Al site, relaxation effects around substituted Cr may be similar in both structures. The cation-oxygen distances of the host site do not explain the low crystal field values, as the Al site is smaller in variscite and metavariscite than in most anhydrous silicates and oxides (e.g., Burns 1993). Such a weak crystal field splitting may originate from the low effective charge of the phosphate ligands, although the actual Cr-O distances have not been determined in variscite. The association with  $\text{PO}_4$  groups of 4 of the 6 oxygen neighbors of  $\text{Cr}^{3+}$  in variscite and metavariscite gives these oxygen atoms a low effective charge, in contrast to simple oxides and hydrated complexes. However, the crystal field splitting values are higher than in phosphate glasses, in which they are as low as  $1450\text{ cm}^{-1}$  (Lempicki et al. 1980). This may arise from the additional presence of two  $\text{H}_2\text{O}$  ligands around  $\text{Cr}^{3+}$  in variscite. Indeed, the crystal field splitting parameter increases in the presence of  $\text{H}_2\text{O}$  and  $\text{OH}^-$  ligands (Platonov et al. 1996), as shown by systematic studies of the spectrochemical series: by comparison,  $\text{Cr}(\text{H}_2\text{O})_6^{3+}$  complexes show a  $Dq$  value of  $1740\text{ cm}^{-1}$  (Burns 1993).

The influence of the distortion of the substituted Al-site is reflected in the diffuse reflectance spectra. As indicated above, the  ${}^4A_2 \rightarrow {}^2E_g(G)$  transition in variscite is split into two components, an indication of a local distortion, as the  ${}^2E_g$  level remains unsplit in trigonal distortion in contrast to orthorhombic or lower symmetry. Splitting might be expected to result from Cr substituting in a site characterized by an Al-O distance distribution, the influence of the site distortion on the crystal field splitting being reinforced by the different effective charge between the O atoms belonging to  $\text{PO}_4$  groups and  $\text{H}_2\text{O}$  molecules. In the host structure, O-Al-O angles range between  $83.7$  and  $93.9^\circ$ , an indication of a significant angular distortion of the Al octahedron. By contrast, in metavariscite, there is no apparent splitting of the dip corresponding to the  ${}^4A_2 \rightarrow {}^2E_g(G)$  transition. The absence of splitting of this transition in the metavariscite spectrum indicates that  $\text{Cr}^{3+}$  occupies a more regular octahedron. In the cation host site, O-Al-O angles are less distributed than in variscite, with values ranging between  $86.7$  and  $94.4^\circ$ ; the Cr for Al substitution does not modify the geometry of the Al-substituted site. The  $T_{1g}$  or  $T_{2g}$  levels are also split in orthorhombic and lower symmetries. Despite the fact that the v1 band does not show an apparent splitting in variscite and metavariscite, a small shoulder is observed at about  $21\,000\text{ cm}^{-1}$  on the v2 absorption

band because this band is more sensitive to first-order splitting (Henderson and Imbush 1989).

The Racah parameter  $B$  is a measure of the degree of interelectronic  $d-d$  repulsion and is derived from the following relationship (Burns 1993):

$$B = \frac{1}{3} \frac{(2v_1 - v_2)(v_2 - v_1)}{9v_1 - 5v_2} \quad (4)$$

In variscite, the Racah parameter  $B = 657 \text{ cm}^{-1}$ . This term is reduced by  $\approx 1/3$  of the free ion value ( $1030 \text{ cm}^{-1}$ ). This reduction is higher than when in the presence of  $\text{H}_2\text{O}$  and  $\text{OH}$  ligands, indicating a significantly covalent Cr-O bond in variscite. This value is in the range of that found in most oxide and silicate minerals. The value of  $Dq / B = 2.43$  indicates that  $\text{Cr}^{3+}$  ions occupy weak-field sites, corresponding to the region in which the  ${}^4T_{2g}(F)$ ,  ${}^2E_g(G)$ , and  ${}^2T_{1g}(G)$  levels cross. In metavariscite, although the steep charge transfer absorption edge limits an accurate location of the  $v_2$  band, the  $B$  parameter of  $\text{Cr}^{3+}$  may be estimated to be about  $575 \text{ cm}^{-1}$ . The differences in the  $B$ -value of variscite and metavariscite result from an opposite shift of the  $v_1$  and  $v_2$  absorption bands, which occur at higher and lower wavenumber values, respectively, in metavariscite relative to variscite. The difference between  $B$  Racah parameter values indicates a higher Cr-O bond covalence in metavariscite than in variscite, relative to slightly shorter Al-O distances and a smaller distribution of the Al-O distances. This confirms the similarity of the Cr to Al substitution process in both minerals, which retains some characteristics of the unsubstituted Al site.

### Crystal chemistry of V

In low temperature fluids, V is transported primarily in the 4+ and 5+ oxidation states and occurs in minerals in a wide range of structural units (Schindler et al. 2000). The presence of V as vanadate groups, which may substitute for  $\text{PO}_4$  tetrahedra, may contribute significantly to the intense charge transfer located in the ultraviolet and extending into the violet end of the visible region. Second, the absorption band around  $12000 \text{ cm}^{-1}$ , due to the vanadyl groups, has a weak intensity relative to that of the  $\text{Cr}^{3+}$  absorption bands, which is in agreement with the low  $\text{V}^{4+}$  concentration detected by EPR spectra. The presence of these vanadyl groups substituting for the  $\text{AlO}_4(\text{H}_2\text{O})_2$  octahedra is then not responsible for the coloration of variscite.

The EPR parameters give a detailed description of the local geometry around the vanadyl groups, as the value of  $g_{\parallel}$  increases with the tetragonal distortion and exceeds that of  $g_{\perp}$ . The values found in the Pannecé sample are similar to those of  $\text{VO}(\text{H}_2\text{O})_5^{2+}$  complexes and  $\text{AlPO}_4:\text{V}$  molecular sieves, and to a lesser extent to  $\text{V}^{4+}$ -doped hexahydrate phosphates (see, e.g., Shiyamala et al. 2002). In V-bearing  $\text{AlPO}_4$  molecular sieves, V occurs at octahedral sites, characterizing a  $\text{VO}(\text{H}_2\text{O})_3^{2+}$  complex coordinated to two framework oxygen atoms bonded to Al (Blasco et al. 2000; Frunza et al. 2000). In a vanadyl hydrate complex, the  $\text{V}^{4+}$  cation is displaced from the center of the octahedron toward one apex O atom. The site is characterized by a short vanadyl bond ( $<1.62 \text{ \AA}$ ), four equatorial V-O distances in the plane perpendicular to the vanadyl bond at  $1.85\text{--}2 \text{ \AA}$ , and a longer V-O bond ( $>2.20 \text{ \AA}$ ) opposed to the vanadyl bond, a geometry which is also found in anhydrous phosphates, as shown recently in

phosphovanadylite (Medrano et al. 1998). This axially distorted surrounding of the  $\text{V}^{4+}$  cation helps to minimize site relaxation during substitution of this ion at the Al octahedral site. Indeed, the local surrounding of V is more regular in variscite than in V-bearing aluminophosphates (Blasco et al. 2000). The high value of the  $A_{\parallel}$  hyperfine parameter indicates an ionic character of the equatorial  $\text{V}^{4+}$ -O bonds.

Vanadium geochemistry is sensitive to environmental conditions such as acidity and oxidation. In low temperature environments, pentavalent V is the most stable oxidation state inoxic waters, accounting for its dominant role in the crystal chemistry of low temperature V minerals. Vanadyl complexes are restricted to reducing conditions and their oxidation rate is enhanced by the presence of oxide surfaces (Wehrli and Stumm 1989). Due to the low concentration of  $\text{V}^{4+}$  detected by EPR, the samples of variscite investigated formed under oxidizing conditions, in the absence of  $\text{Fe}^{2+}$  and  $\text{V}^{3+}$  ions. The weakness of the EPR signal in metavariscite, which is the most V-rich sample, shows that vanadium occurs mostly as vanadate in this sample, an indication of more oxidizing conditions of formation.

### ACKNOWLEDGMENTS

We thank M. Fialin (CAMPARIS, University of Paris VI, France) for help with the electron microprobe measurements. We acknowledge J.-C. Boulliard, B. Lasnier, C. Derré, and M. Lecolle for providing us with the samples investigated in this study. We thank H. Halenius, J. Hanchar, and an anonymous reviewer for their comments on this paper. This is IPGP Contribution 2035.

### REFERENCES CITED

- Amthauer, G. and Rossman, G.R. (1984) Mixed valence of iron in minerals with cation clusters. *Physics and Chemistry of Minerals*, 11, 37–51.
- Babonneau, F., Sanchez, C., Livage, J., Launay, J.P., Daoudi, M., and Jeannin, Y. (1982) Spectroscopic study of mixed valence complexes between  $\text{V}^{\text{IV}}$  and  $\text{V}^{\text{V}}$ . *Nouveau Journal de Chimie*, 6, 353–357.
- Balan, E., Allard, T., Morin, G., and Calas, G. (2002) Incorporation of  $\text{Cr}^{3+}$  in dickite: a spectroscopic study. *Physics and Chemistry of Minerals*, 29, 273–279.
- Ballhausen, C.J. and Gray, H.B. (1962) The electronic structure of the vanadyl ion. *Inorganic Chemistry*, 1, 111–122.
- Blasco, T., Fernández, L., Martínez-Arias, A., Sánchez-Sánchez, M., Concepción, P., and López Nieto, J.M. (2000) Magnetic resonance studies on V-containing, and V,Mg-containing AFI aluminophosphates. *Microporous and Mesoporous Materials*, 39, 219–228.
- Burns, R.G. (1993) *Mineralogical applications of crystal field theory*, 2nd ed., 574 p. Cambridge University Press, Cambridge.
- Calas, G. (1988) Electron paramagnetic resonance. In F.C. Hawthorne, Ed., *Spectroscopic Methods in Mineralogy and Geology*, 18, 513–571. Reviews in Mineralogy, Mineralogical Society of America, Washington, D.C.
- Calas, G., Manceau, A., Novikoff, A., and Boukili, H. (1984) Comportement du chrome dans les minéraux d'altération du gisement de Campo-Formoso (Bahia, Brésil). *Bulletin de Minéralogie*, 107, 755–766.
- Catana, G., Rao, R.R., Weckhuysen, B.M., Van Der Voort, P., Vansant, E., and Schoonheydt, R.A. (1998) Supported V oxide catalysts: Quantitative spectroscopy, preferential adsorption of  $\text{V}^{4+}/\text{V}^{5+}$ , and  $\text{Al}_2\text{O}_3$  coating of zeolite Y. *Journal of Physical Chemistry B*, 102, 8005–8012.
- Damour, A. (1864) Sur la Callaïs, nouveau phosphate d'alumine hydraté recueilli dans un tombeau celtique du Morbihan. *Comptes Rendus des Séances de L'Académie des Sciences de Paris*, V, 936–940.
- Forestier, F.H., Lasnier, B., and L'Helgouach, J. (1973) Découverte de minyulite en échantillons spectaculaires, de wavellite et de variscite dans des phanites siluriens près de Pannecé (Loire-Atlantique). *Bulletin de la Société française de Minéralogie et Cristallographie*, 96, 67–71.
- Foster, M.D. and Schaller, W.T. (1966) Cause of color in wavellite from Dug Hill, Arkansas. *American Mineralogist*, 51, 422–428.
- Fritsch, E. and Rossman, G.R. (1987) An update on color in gems. Part 1: Introduction and colors caused by dispersed metal ions. *Gemst and Gemology*, 23, 126–139.
- Frunza, L., Van Der Voort, P., Vansant, E.F., Schoonheydt, R.A., and Weckhuysen, B.M. (2000) On the synthesis of V containing molecular sieves by experimental design from a  $\text{VOSO}_4 \cdot 5\text{H}_2\text{O} \cdot \text{Al}(\text{iPrO})_3 \cdot \text{Pr}_2\text{NH} \cdot \text{H}_2\text{O}$  gel: occurrence of VAP-41 as a secondary structure in the synthesis of VAP-11. *Microporous, and Mesoporous Materials*, 39, 493–507.

- Garcia-Guinea, J., Sapalski, C., Cardenes, V., and Lombardero, M. (2000) Mineral inlays in natural stone slabs: techniques, materials and preservation. *Construction and Building Materials*, 14, 365–373.
- Gupta, S., Khanijio, N., and Mansingh, A. (1995) The influence of  $V^{4+}$  ion concentration on the EPR spectra of vanadate glasses. *Journal of Non-Crystalline Solids*, 181, 58–63.
- Hapke, B. (1993) *Introduction to the Theory of Reflectance and Emittance Spectroscopy*. Cambridge University Press, New York.
- Henderson, H. and Imbush, G.F. (1989) *Optical Spectroscopy of Inorganic Solids*. Oxford Science, New York.
- Kniep, R. and Mootz, D. (1973) Metavariscite- A redetermination of its crystal structure. *Acta Crystallographica*, B29, 2292–2294.
- Kniep, R., Mootz, D., and Vegas, A. (1977) Variscite. *Acta Crystallographica*, B33, 263–265.
- Larsen, E.S. (1942) The mineralogy and paragenesis of the variscite nodules from near Fairfield, Utah. Part 3. *American Mineralogist*, 27, 441–451.
- Lempicki, A., Andrews, L., Nettel, S.J., McCollum, B.C., and Solomon, E.I. (1980) Spectroscopy of  $Cr^{3+}$  in glasses: Fano antiresonances and vibronic Lamb shift. *Physical Review Letters*, 44, 1234–1237.
- Malengreau, N., Muller, J.P., and Calas, G. (1994) Fe-speciation in kaolins: a diffuse reflectance study. *Clays and Clay Minerals*, 42, 137–147.
- Manceau, A. and Calas, G. (1985) Heterogeneous distribution of nickel in hydrous silicates from New Caledonia ore deposits. *American Mineralogist*, 70, 549–558.
- Marty, J., Howard, D.G., and Barwood, H. (1999) Minerals of the Utahlite Claim, Lucin, Box Elder County, Utah, 13 pp. Utah Geological Survey Miscellaneous Publication 99–6.
- Medrano, M.D., Evans, H.T. Jr., Wenk, H.R., and Piper, D.Z. (1998) Phosphovanadylite: A new V phosphate mineral with a zeolite-type structure. *American Mineralogist*, 83, 889–895.
- Meireles, C., Ferreira, N., and Reis, M.L. (1987) Variscite occurrence in Silurian formations from northern Portugal, *Comunicações dos Serviços Geológicos de Portugal*, 73, 21–27.
- Muller, J.P., Manceau, A., Hazemann, J.L., Allard, T., Ildefonse, Ph., and Calas, G. (1995) Crystal chemistry of clays and associated oxides: constraints for modeling element transfer at the Earth's surface. *American Journal of Science*, 295, 1115–1155.
- Pavlov, R.S., Marza, V.B., and Carda, J.B. (2002) Electronic absorption spectroscopy and colour of chromium-doped solids. *Journal of Materials Chemistry*, 12, 2825–2832.
- Platonov, A.N., Langer, K., Andrut, M., and Calas, G. (1996)  $Cr^{3+}$  in phyllosilicates: influence of the nature of coordinating ligands and their next cationic neighbors on the crystal field parameters. In M.D. Dyar, C. McCammon, and M.W. Schaefer, Eds., *Mineral spectroscopy: A tribute to Roger G. Burns*. The Geochemical Society Special Publication no. 5, 41–48.
- Rossmann, G.R. (2004) Mineral Spectroscopy Server, California Institute of Technology, Pasadena, California, U.S.A. <http://minerals.gps.caltech.edu/FILES/Visible/Variscite/Index.htm>
- — — (1988) Optical Spectroscopy. In F.C. Hawthorne, Ed., *Spectroscopic Methods in Mineralogy and Geology*, 18, 207–254. Reviews in Mineralogy, Mineralogical Society of American, Washington, D.C.
- Ruitenbeek, M. (1998) Characterisation of Vanadium-Based Oxidation Catalysts. Ph.D. Thesis, University of Utrecht.
- Salvador-Salvador, P. and Fayos, J. (1972) Some aspects of the structural relationship between “Messbach-type” and “Lucin-type” variscites. *American Mineralogist*, 57, 36–44.
- Schindler, M., Hawthorne, F.C., and Baur, W.H. (2000) A crystal-chemical approach of the composition and occurrence of V minerals. *Canadian Mineralogist*, 38, 1443–1456.
- Sheridan, A. (2000) Achnacreebeag and its French connections: Vive the ‘auld alliance’. In J.C. Henderson, Ed., *The Prehistory and Early History of Atlantic Europe*, p. 1–15. BAR International Series 861. Oxford.
- Shiyamala, C., Rajendiran, T.M., Venkatesan, R., and Rao, P.S. (2002) Host lattice effect on paramagnetic impurity: single crystal EPR study of VO(II)-doped biomimetic cadmium ammonium phosphate hexahydrate. *Crystal Research Technology* 37, 841–848.
- Siegel, I. (1964) Paramagnetic resonance of V in amorphous and polycrystalline  $GeO_2$ . *Physical Review*, 134, A193–A197.
- Villalba, M.J. (2002) Le gîte de variscite de Can Tintorer: Production, transformation, et circulation du minéral vert. In J. Guilaine, Ed., *Matériaux, productions, circulations du Néolithique à l’âge du bronze*, Paris: Éditions Errance, p. 115–129.
- Wehrli, B. and Stumm, W. (1989) Vanadyl in natural waters: adsorption and hydrolysis promote oxygenation. *Geochimica et Cosmochimica Acta*, 53, 69–77.

MANUSCRIPT RECEIVED APRIL 8, 2004

MANUSCRIPT ACCEPTED OCTOBER 29, 2004

MANUSCRIPT HANDLED BY JOHN HANCHAR